Crystalline Morphology of PLA/Clay Nanocomposite Films and Its Correlation with Other Properties

Kunal Das,[1] Dipa Ray,[1] Indranil Banerjee,[1] N. R. Bandyopadhyay,[2] Suparna Sengupta,[3] Amar K. Mohanty,[4] Manjusri Misra[5]

[1]*Department of Polymer Science & Technology, University of Calcutta, Kolkata, West Bengal 700009, India*
[2]*School of Materials Science and Engineering, Bengal Engineering and Science University, Shibpur, Howrah 711103, India*
[3]*Indian Association for the Cultivation of Science, Kolkota, West Bengal 700032, India*
[4]*Bioproducts Discovery and Development Centre, Department of Plant Agriculture, Crop Science Building, University of Guelph, Guelph N1G2W1, ON, Canada*
[5]*School of Engineering, Thornbrough Building, University of Guelph, Guelph N1G2W1, ON, Canada*

Received 25 August 2009; accepted 24 February 2010
DOI 10.1002/app.32345
Published online 14 May 2010 in Wiley InterScience (www.interscience.wiley.com).

ABSTRACT: Polylactic acid (PLA)-based composite films with four different loadings of nanoclay (2, 5, 10, and 15 wt %) were prepared using a solvent casting method and their crystalline morphology was investigated. The crystalline morphology was significantly different in the films depending on the clay content and its dispersion in the matrix. The clay platelets played the role of nucleating sites facilitating crystallization during solvent evaporation and this effect was most predominant in PLA 10. The % crystallinity and the crystallite size were determined by XRD analysis. The morphology was investigated with scanning electron microscopy (SEM) and by atomic force microscopy (AFM). A fibrillar pattern was evident in SEM micrographs, which were confirmed by AFM. The thermal properties were investigated with DSC and TGA. The glass transition temperature (T_g) increased from 51.9 to 55–57°C in all the nanocomposite samples. The melting peak temperature (168°C) remained unaltered in the nanocomposites, but the melting enthalpy varied depending on the PLA/clay interaction. The rate of degradation was controlled by the dispersion of clay platelets in the matrix and was very low in low clay-filled films. © 2010 Wiley Periodicals, Inc. J Appl Polym Sci 118: 143–151, 2010

Key words: biodegradable polymers; clay; electron microscopy

INTRODUCTION

Polylactic acid (PLA) is biodegradable and biocompatible thermoplastic polyester produced from renewable resources. PLA can be used in various fields, such as industrial packaging, biomedical applications, such as tissue engineering, drug delivery, dental, and so on. For some applications, PLA need to be modified for enhanced mechanical properties, barrier property, higher thermal stability, and so on. PLA/clay nanocomposites have already gained a big popularity among the material scientists because of their exceptional properties, which are superior to the virgin polymer in many ways. The nanostructure formed can be tailored by changing the type of nanoclay used, by changing their preparation method, by varying the clay loading, and by controlling the clay dispersion. PLA/clay nanocomposites have been prepared by several methods, such as melt extrusion and solution casting.[1] Shibata et al.[2] prepared PLA/organoclay nanocomposites by melt mixing in presence of plasticizer and reported improved mechanical properties. They also observed an increase in crystallization because of incorporation of plasticizers because of increase in PLA chain mobility. Maiti et al.[3] investigated the roles of different types of clays (smectite, mica, and momontmorillonite) in PLA/clay nanocomposites. Hasook et al.[4] conducted research on PLA/clay nanocomposites by melt compounding. They observed that tensile strength, modulus and elongation at break increased significantly on addition of clay in the PLA matrix. Ray et al.[5] reported that type of clay dispersion affected the physical and morphological properties of the composites. Natalia et al.[6] conducted research on PLA/clay nanocomposites and observed morphologically different network structures of the processed nanocomposites. Cava et al.[7] observed that PLA nanocomposite film showed higher barrier property than PLA blank film. Ray et al.[8] reported the detailed melt rehological

Correspondence to: D. Ray (roy.dipa@ gmail.com).
Contract grant sponsors: AICTE (All India Council for Technical Education, Government of India), DST (Government of India), University of Guelph, The Ontario Ministry of Agriculture, Food and Rural Affairs (OMAFRA) 2008 Bioproducts Research Program.

Journal of Applied Polymer Science, Vol. 118, 143–151 (2010)

properties of C_{18}-MMT based PLA nanocomposites. In another study, they have reported the control of biodegradability of polylactide via nanocomposite technology.[9] They described a novel nanocomposite approach for polylactide that resulted in a nanoscale control of the biodegradability of polylactide under compost. Crystallization behavior and morphology of biodegradable polylactide/layered silicate nanocomposites were reported by Nam et al.[10] They observed that overall crystallization rate of neat PLA increased after nanocomposite formation without influencing the linear growth rate of pure PLA.

Tensile, water vapor barrier, and antimicrobial properties of PLA/nanoclay composite film were extensively studied by Rhim et al.[11] They reported that dispersion and concentration of nanoclays played an important role for property modification. The crystallization behavior of PLA nanocomposites, nucleation, and growth probed by infrared spectroscopy were reported by Krikorioan et al.[12] Morphology and properties of polylactide modified by thermal treatment, filling with layered silicates and plasticization was reported by Pluta.[13] The influence of composition and heat treatment on the structure and physical properties, such as crystallization behavior, viscoelastic property, and so on, were elaborately explained by him. The structural, thermal, and mechanical properties of PLA/clay blend were reported by Ogata et al.[14] Cold crystallization and the role of clay particles as a nucleating agent were also reported by them.

The properties of nanocomposites and their rates of biodegradation strongly depends on their crystal structure and morphology. This large influence of crystal structure development and resulting morphology on all properties of the nanocomposites encouraged us to carry out this research work. This contribution reports the preparation of PLA/clay nanocomposite film by solution blending technique. Keeping all the processing parameters constant, the clay loading was varied from 2 to 15 wt %. The resulting crystallinity and morphology of the films were investigated by XRD, scanning electron microscope (SEM), and atomic force microscopy (AFM). FTIR was done to determine the differences in structures of the films. The variation in properties was investigated by DSC and TGA.

EXPERIMENTAL

Materials

PLA (Nature works, PLA Polymer 3001 D) was used as matrix material. Chloroform (Merck) was used as the solvent for PLA. Cloisite 30B was used as the organoclay (Southern Clay Products).

Preparation of films

A calculated amount of PLA was dissolved in chloroform to prepare a clear solution of PLA. Then a measured amount of organoclay (Cloisite 30B) was added to the PLA solution and sonicated for 1 h for good dispersion of clay in the PLA solution. Then the PLA/clay solution was cast on polypropylene trays and petri dishes. Five sets of films were prepared with 0, 2, 5, 10, and 15 wt % of nanoclay loading and were named as PLA 0, PLA 2, PLA 5, PLA 10, and PLA 15, respectively.

Characterization

X-ray diffraction studies of the samples were carried out by high-resolution X-ray diffractometer (X'Pert PRO) Model RIGAKU MINISLEX with a scanning rate of 4°/min with CuKa radiation operating at 45 KV and 40 mA within a scan range of $2\theta = 2°–35°$. AFM was done with AFM Model: Veeco multimode Nanoscope IIIa with a tapping mode. The surface

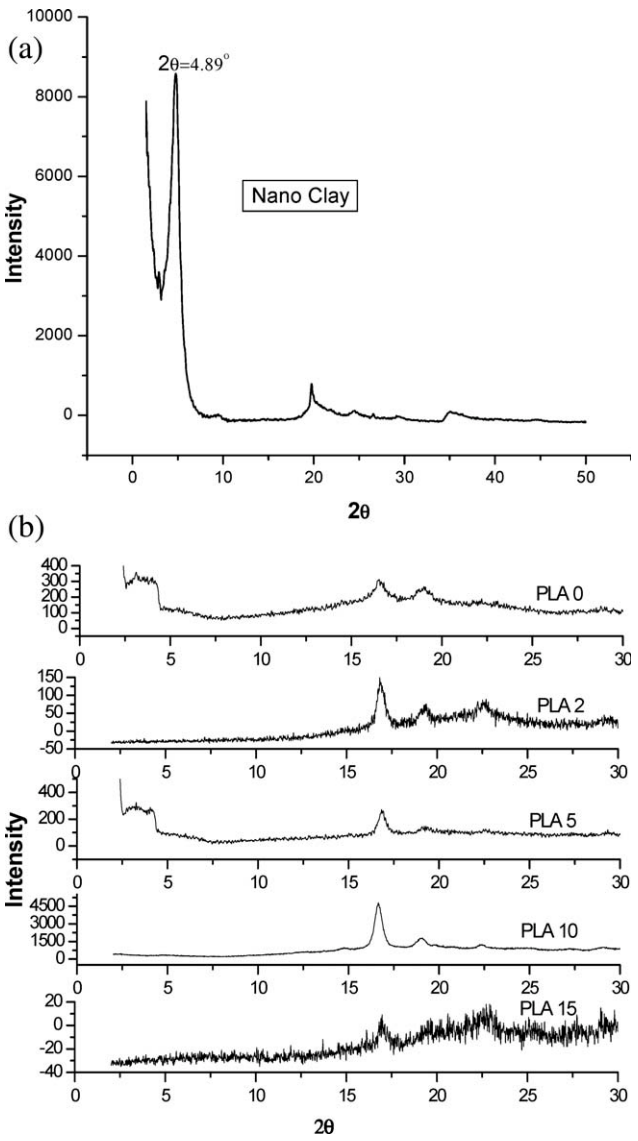

Figure 1 XRD graph of the (a) organoclay, (b) PLA/clay nanocomposite films in the range $2\Theta = 2–35°$.

TABLE I
% Crystallinity and Crystallite Size of PLA Nanocomposites with Respect to 200 Plane Reflection

Sample ID	Crystallite size (nm)	% Crystallinity
PLA 0	14.21	38.94
PLA 2	19.07	71.98
PLA 5	19.32	66.35
PLA 10	16.85	83.70
PLA 15	17.46	65.40

morphology of the film samples were investigated under LEICA S 440 SEM, using a voltage of 20 kV by coating with Au-Pd alloy. ATR-IR analysis was done with FTIR-8300 SHIMADZU. DSC analysis was carried out with Perkin Elmer Diamond DSC in the temperature range 0–200°C with a heating rate 5°C/min. Thermogravimetric analysis (TGA) of the PLA/clay films was done with TGA-Model Pyris Diamond TGA/DTA (Perkin Elmer) with a heating rate of 5°C/min in nitrogen atmosphere.

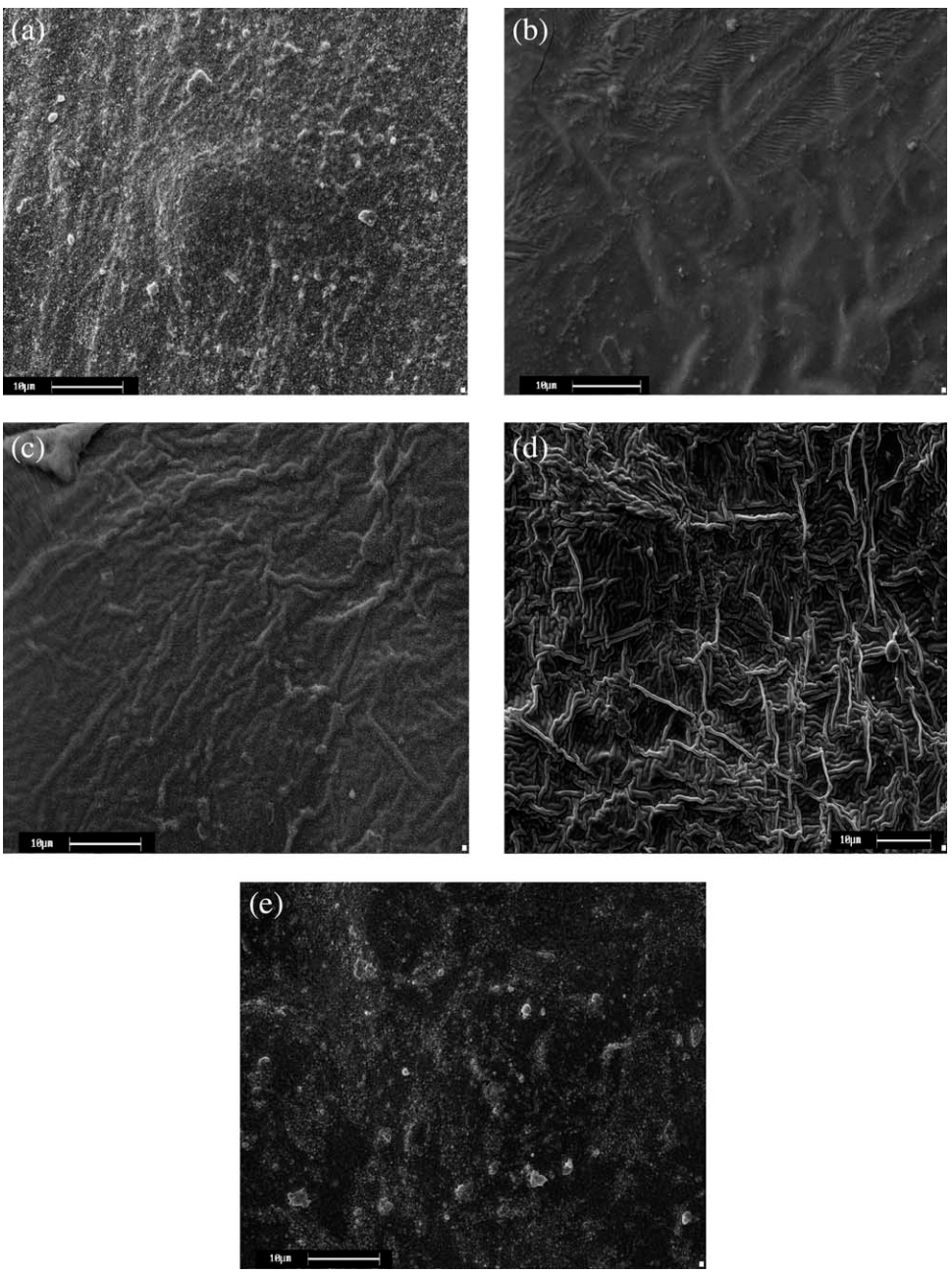

Figure 2 (a) Surface morphology of PLA 0. (b) Surface morphology of PLA 2 showing minor fibrillar pattern. (c) Surface morphology of PLA 5 exhibiting a prominent fibrillar pattern. (d) Distinctive fibrils observed in PLA 10. (e) Diffused morphology in PLA 15.

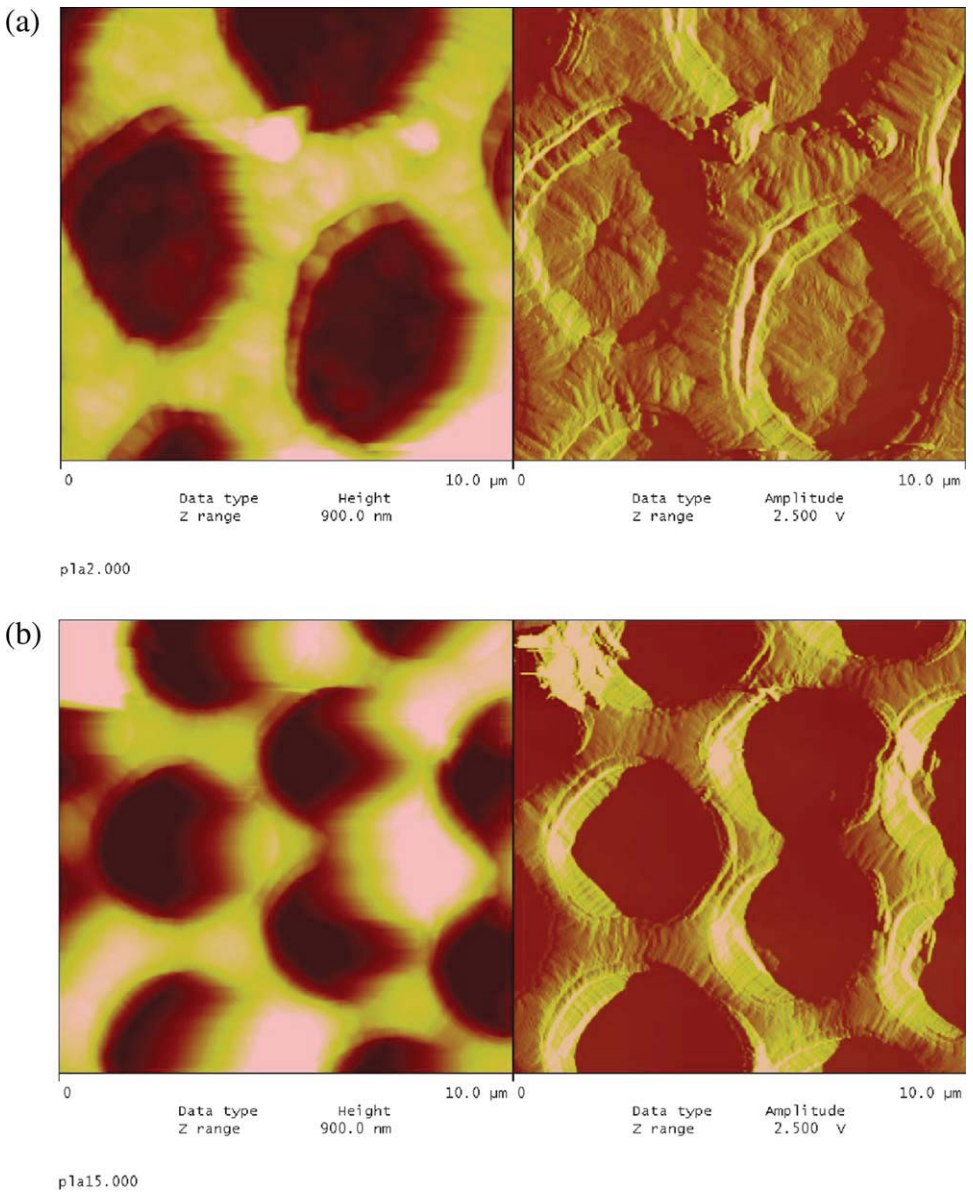

Figure 3 Surface morphology of (a) PLA 2 and (b) PLA 15 by AFM showing "hole-rim" pattern. [Color figure can be viewed in the online issue, which is available at www.interscience.wiley.com.]

RESULTS AND DISCUSSION

The XRD patterns of nanoclay (Cloisite 30B) and nanocomposites (PLA 0, PLA 2, PLA 5, PLA 10, and PLA 15) are shown in Figure 1(a,b), respectively. The cloisite 30B peak ($2\Theta = 4.89°$),[15] shown in Figure 1(a), was not observed in any of the composite samples [Fig. 1(b)], indicating exfoliation. An intensive peak was observed at 16.6° and two small peaks were observed at 19.3° and 22.9°. The 16.6° peak could be assigned to the (200) and/or (110) plane of typical orthorhombic crystal.[16] The small peaks at 19.3° and 22.9° appeared because of the reflection from (203) and (105) planes, respectively.[10]

The crystallite size was calculated by using the Scherrer equation,

$$L_{h,k,1} = K\,\lambda/\beta\cos\theta \qquad (1)$$

where, $K = 0.94$,[17] based on the full width at half maximum of 101 and 002 reflections. The % crystallinity was also calculated as per the formula,[18]

$$\%\text{Crystallinity} = (I_{200} - I_{am})/I_{200} \times 100 \qquad (2)$$

In PLA 0, the peak at $2\Theta = 16.6°$ exhibited low intensity and the crystallite size was 14.21 nm. But for PLA/clay nanocomposite films, the peaks became sharper and the crystallite sizes were increased, indicating a more ordered structure.[3] When organoclay was dispersed in PLA solution in chloroform by sonication, the PLA chains could easily penetrate in

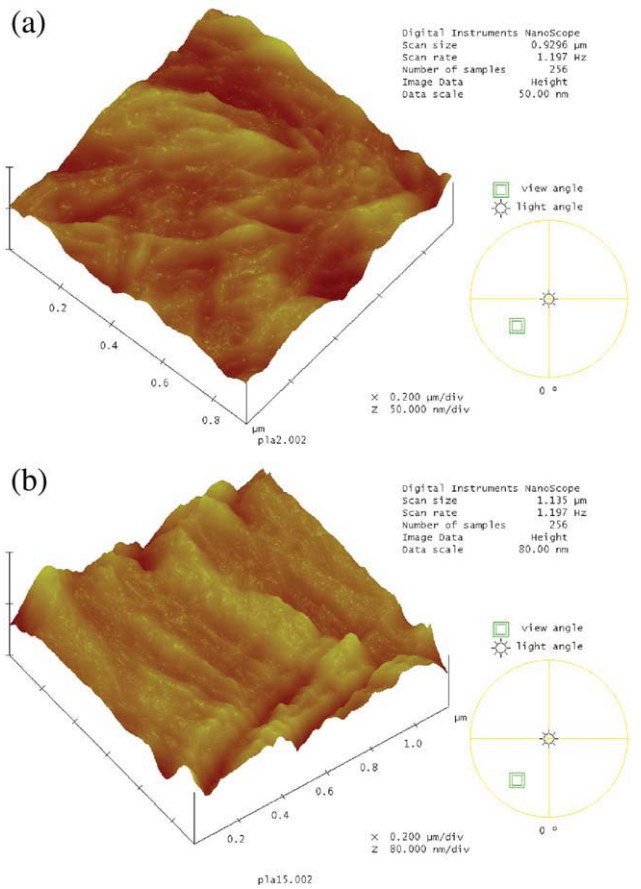

Figure 4 3D Surface of (a) PLA 2 and (b) PLA 15 nanocomposite by AFM. [Color figure can be viewed in the online issue, which is available at www.interscience.wiley.com.]

between the clay platelets causing exfoliation. As the solvent-cast films were dried at room temperature, the PLA chains had sufficient time to rearrange themselves around the dispersed clay platelets. There might be association of several individual chains around these clay platelets increasing the overall crystallinity of the samples. The % crystallinity and crystallite size of the samples are given in Table I. The amount of clay and their extent of dispersion changed the crystallization behavior of the films. Ogata et al.[14] also reported that clay acted as nucleating agent in PLA/clay nanocomposite films. The intensities of the three XRD peaks changed considerably in the nanocomposite films, which show that different clay loading controlled the molecular packing significantly.

In PLA 2, the distance between the dispersed platelets was quite high to accommodate a larger number of polymer chains around it. So the crystallite size (19.07 nm) and % crystallinity (71.9%) with respect to 200 planes increased compared with that of PLA 0. The XRD curve also showed emergence of two small peaks at 19.3° and 22.9°, which appeared because of diffraction in 203 and 105 planes. This indicates that the nanoclay was dispersed uniformly throughout the matrix and initiated crystallization in different planes. The crystallite size (19.32 nm) increased in PLA 5, compared with that of PLA 0, but % crystallinity with respect to 200 plane decreased slightly (66%). No other XRD peak was evident, which indicates formation of ordered regions perpendicular to 200 plane only.

In PLA 10, the crystallite size was smaller (16.85 nm) than PLA 2 and PLA 5 and the % crystallinity with respect to 200 plane increased to 81%. It indicates that in PLA 10, a larger number of finer crystallites were formed perpendicular to 200 plane and increased the crystallinity of the film. Two very small but distinctly visible peaks were observed at 19.3° and 22.6°. In PLA 15, crystallite size was found to be 17.46 nm, and the crystallinity was lowered (65%). The intensity of peak increased significantly at 22.7° indicating the formation of crystalline regions perpendicular to 105 planes.

The exfoliated silicate layers provide large surface area because of their nanosize and act as nucleating sites facilitating the crystallization behavior. With the increase of clay content, the nucleating sites also increased, but at the same time, high miscibility between the organomodifier and the polymer chains immobilized the polymer chains and obstructed them from taking part in the flow during the crystallization process. Thus, two opposite phenomenon were acting simultaneously.[1,19]

The increase in % crystallinity and crystallite size in PLA 2 compared with that of PLA 0 indicates that addition of 2 wt % clay facilitated the crystallization process. But in PLA 5, the interaction between the polymer chains and the alkyl groups of the organomodified clays might be predominant, which restricted the motion of the polymer chains and obstructed them from taking part in crystallization process. In PLA 10, nucleating effect of clay might be predominant, which facilitated the crystallization process. Thus, PLA 10 exhibited highest % crystallinity (83.7%) and lower crystallite size. In PLA 15, crystallinity dropped to 65%, which can be ascribed to the strong opposing phenomenon acting between the miscibility and nucleation effects.

The surface morphology of the PLA 0, PLA 2, PLA 5, PLA 10, and PLA 15 films were examined under SEM and are shown in Figure 2(a–e), respectively. In PLA 0, the surface exhibited a rough morphology, which might be because of evaporation of solvent from this surface. This roughness appeared in all the films, but distinct fibrillar patterns were evident in the clay loaded films only, except PLA 15, where, a diffused morphology was observed. In PLA 2, PLA 5, and PLA 10, the fibril thickness varied significantly depending on the interactive dominance of one factor over another.

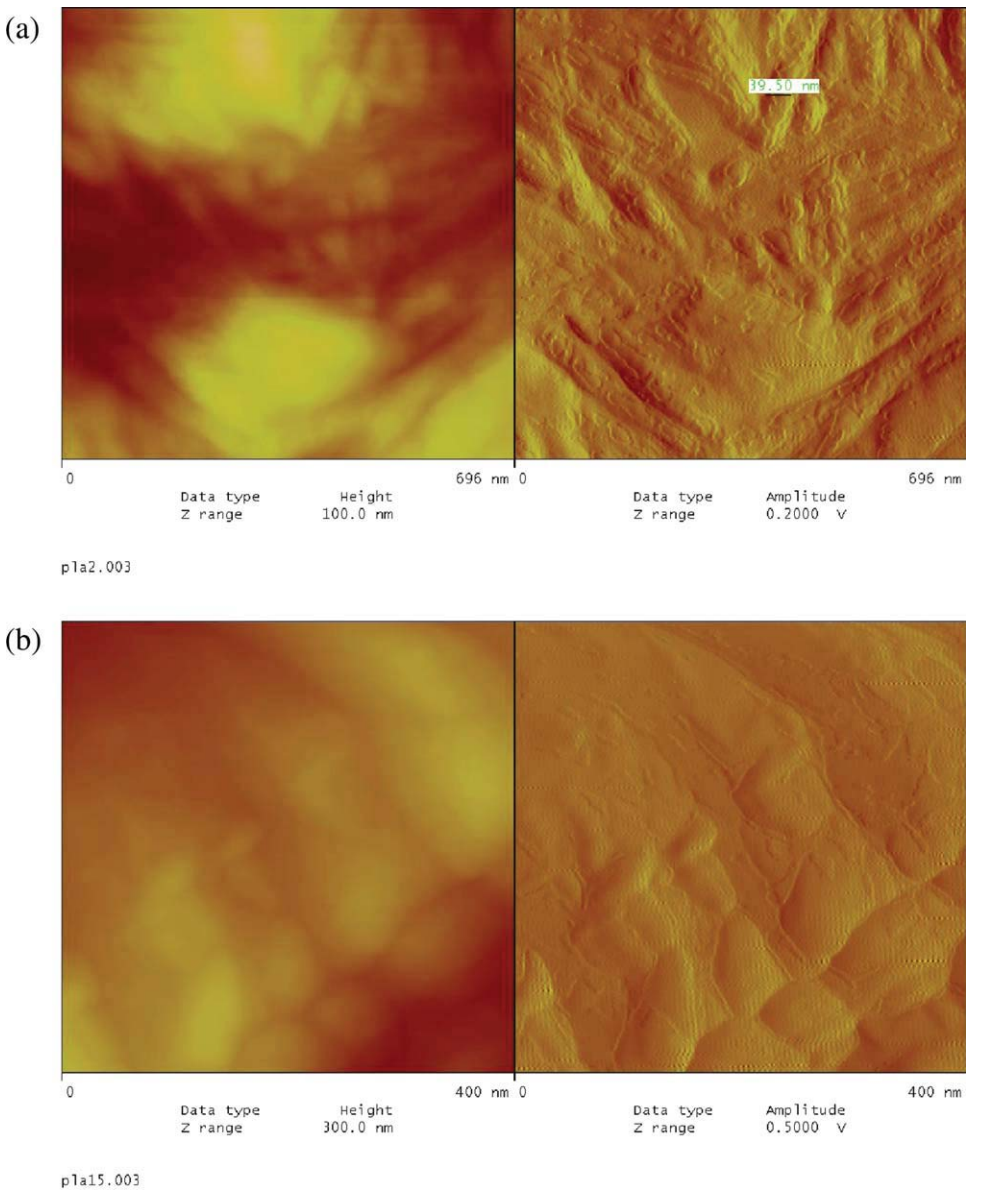

Figure 5 Surface feature of (a) PLA 2 showing fine fibrillar pattern and (b) smooth surface of PLA 15 as observed by AFM. [Color figure can be viewed in the online issue, which is available at www.interscience.wiley.com.]

The AFM images of PLA 2 and PLA 15 nanocomposite films are shown in Figures 3–5. Figure 3 reveals that the chains relaxed forming 'hole-rim' morphology on evaporation of the solvent during AFM test.[20] Thin fibrils, formed at the edge of the holes due to crystallization-induced chain diffusion, were more prominent in PLA 2 than that in PLA 15 (Fig. 3).[21] In the three dimensional picture (Fig. 4), distinct fibrillar pattern is visible in PLA 2 [Fig. 4(a)], but not in PLA 15 [Fig. 4(b)]. In Figure 5 also, a fibrillar morphology was observed in PLA 2. The fibril width was $\sim$ 39 nm [Fig. 5(a)]. But in PLA 15, no such morphology was evident and the surface appeared smooth. This fully corroborated with the SEM observations.

Figure 6 shows the ATR-IR graphs of the nanocomposite samples obtained by taking PLA0 as the

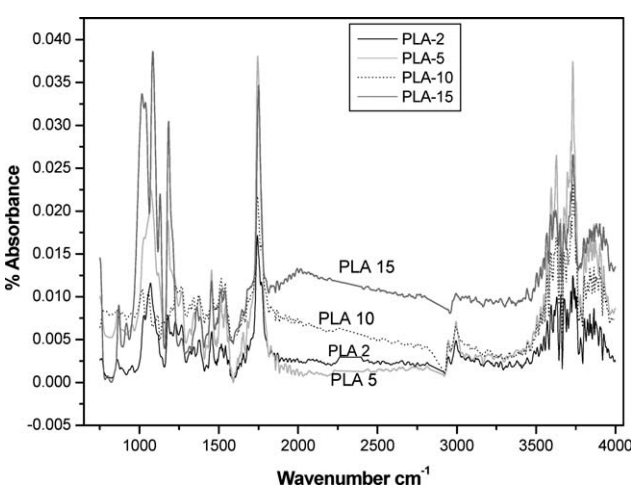

Figure 6 FTIR graph of the PLA/clay nanocomposites.

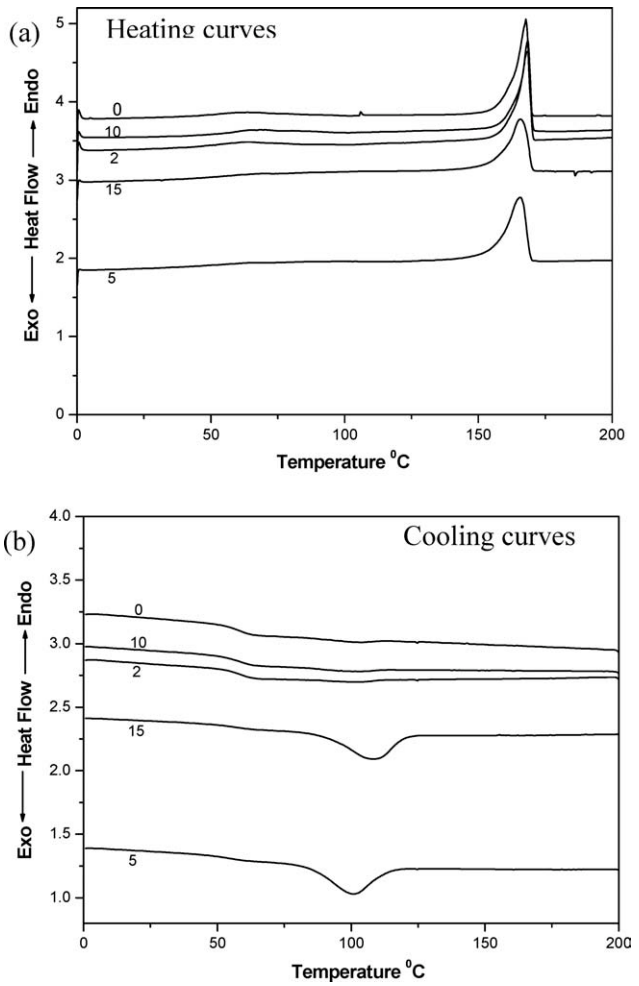

Figure 7 DSC (a) heating and (b) cooling curves of PLA/clay nanocomposites.

reference sample. All the samples exhibited mid-IR regions which are extremely sensitive to structural changes during crystallization.[12] In all PLA/clay nanocomposite samples two consecutive bands appeared in the range 1010–1275 cm^{-1}. These peaks were because of unsymmetrical stretching of —C—O—C— bond. Because of incorporation of clay particles, the rearrangement of PLA chains became more compact. The peak at 1069 cm^{-1} in PLA 2 and at 1018 cm^{-1} in PLA 10 exhibited very low intensity, which can be attributed to the high crystallinity of these samples. In PLA 5 the peak at 1069 cm^{-1} was very sharp and PLA 15 showed two peaks at 1018 cm^{-1} and 1087 cm^{-1} of very high intensity. Emergence of such sharp peaks in PLA 5 and PLA 15 might be because of lower crystallinity of these samples, which allowed free vibrations. The peak appearing at 840 cm^{-1} was because of —C—H out of plane bending. The intensity of this peak was much less in PLA 2 and PLA 10 and was high in PLA 5 and PLA 15. All these results fully corroborate with the XRD observations.

Figure 7 represents the DSC curves of the nanocomposites. The glass transition temperature (T_g) increased from 51.9°C to 55–57°C in all the nanocomposite samples, which can be attributed to the restricted segmental motions of the PLA chains at polymer-clay interface. The chain mobility might also be hindered because of intermittent presence of newly generated crystallites. In all samples, an endothermic melting peak was observed at ~ 168°C, which revealed that incorporation of clay did not much affect the melting temperature of the nanocomposites. The melting enthalpy values indicated probable PLA/clay interactions, which can be well correlated with the XRD observations (Table II). The melting enthalpy was found to be highest in PLA 5 (47.6J/g), which could be attributed to the highest PLA/organomodifier interaction, although % crystallinity was less. It is observed in Figure 7(b) that the glass transition was more distinctly visible in PLA 0, PLA 2, and PLA 10 compared with that in PLA 5 and PLA 15. This indicates that the amorphous phase present in PLA 0, PLA 2, and PLA 10 exhibited a sharp glass transition effect without suffering any hindrance. But in PLA 5 and PLA 15, the crystalline and the amorphous phase might be present in such an entangled manner that the glass transition of the amorphous part was not prominent. During cooling operation, only these two samples exhibited melt crystallization while others did not. The close entanglement between the amorphous and the crystalline phase might have facilitated the melt crystallization process in these two sets. These two sets exhibited lowest % crystallinity (66%) compared with other nanocomposite samples (PLA 2, crystallinity 72% and PLA 10, crystallinity 84%). PLA 5 and PLA 15 showed exothermic peaks due to melt crystallization at 100.6 and 107.5°C, respectively. In PLA 15, crystallization began at a higher

TABLE II
DSC Results of PLA Nanocomposites

Sample ID	T_g (°C)	T_m (°C)	ΔH_m (J/gm)	T_c (°C)	ΔH_c (J/gm)
PLA 0	51.9	167.72	44.35	–	–
PLA 2	57.47	168.38	39.74	–	–
PLA 5	55.07	165.68	47.59	100.52	−24.76
PLA 10	57.33	168.56	35.88		
PLA 15	56.13	165.70	37.70	107.93	−23.93

temperature during cooling cycle in presence of higher clay content.

TGA of the film samples was carried out to investigate their thermal degradation behavior. The change in weight of the samples and the rate of degradation with rise in temperature is shown in Figures 8 and 9, respectively. It was observed that all materials were thermally stable in the region below 220°C, which is the normal processing temperature of PLA.[6] The composites were able to maintain more than 80% of their original weight at this temperature. In Figure 8, a slight decrease in weight was observed for all materials below 150°C, which was because of the moisture loss from them. The PLA samples exhibited a major degradation beginning at 280°C and reaching its peak at 356°C. Although the onset of degradation and the peak degradation temperature were almost similar in all the samples, but there was significant difference in the rate of degradation (Fig. 9). The rate of degradation decreased up to 5% clay loading, which could be due to the strong interaction of the PLA chains with the organomodifier. Then, the rate increased sharply in case of PLA 10, followed by PLA 15. This high rate of decomposition of PLA 10 again indicated that the chains had least interaction with the clay and suffered unhindered thermal degradation. This fully corroborates the previous XRD observations. The residue was lowest in PLA 5 due to inefficient barrier effect of the clay platelets, which decreased the diffusion pathway of the combustion by-products and lowered the residue, similar to PLA 0. In PLA 2, the barrier effect might be more effective which delayed the escape of the volatile degradation products and increased the residue.

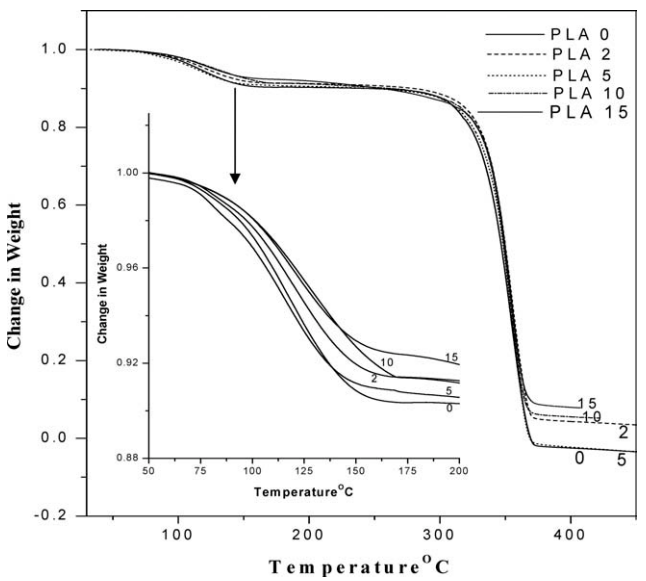

Figure 8 Thermal degradation behavior of PLA nanocomposites.

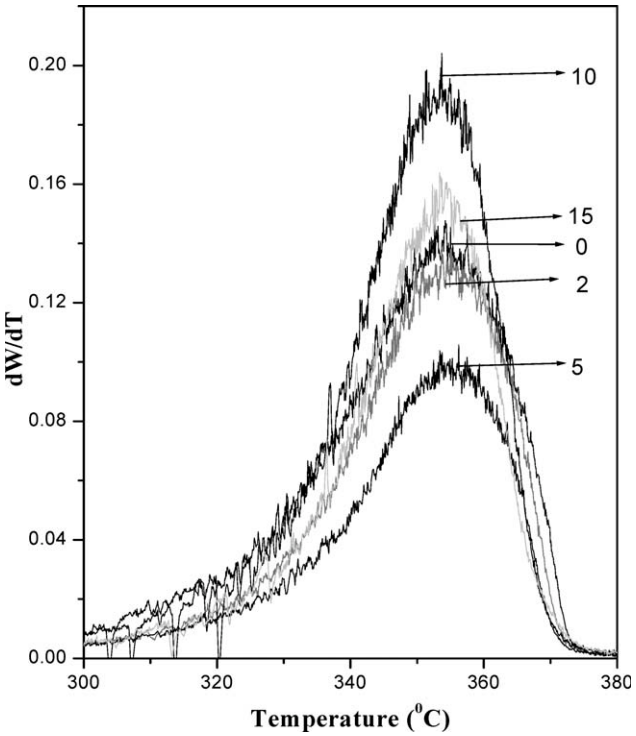

Figure 9 Rate of thermal degradation behavior of PLA nanocomposites.

CONCLUSION

The crystalline morphology of the PLA/clay nanocomposite films were studied and correlated with other properties. XRD observations revealed that organoclay acted as nucleating agents in the nanocomposite films and initiated crystallization. The clay content and clay dispersion controlled the crystalline morphology of the films. A fibrillar morphology became predominant with the increase of clay content up to 10 wt % loading. But in PLA 15, a diffused morphology was evident. It was observed that clay facilitated fibril formation up to 10 wt % loading and beyond that the morphology changed. The T_g of the composite films increased to 57°C compared with that of unreinforced PLA film (51.9°C), indicating hindered chain mobility in presence of dispersed clay platelets. The rate of thermal degradation was slower in low clay loaded film (PLA 2 and PLA 5) because of barrier effect of dispersed clay platelets. But in PLA 10 and PLA 15, the rate of degradation was higher due to presence of ammonium cation, which thermally decomposed to produce ammonia.

Dipa Ray is thankful to *AICTE* (*All India Council for Technical Education*), Government of India, for granting her a project. SSG is grateful to DST, Government of India, for awarding her Research Associateship. AKM and MM are thankful to the 2009 OMAFRA (Ontario Ministry of Agriculture, Food and Rural Affairs) - New Directions & Alternative

Renewable Fuels Research Program Project number SR9225 for the partial financial support to carry out this research.

References

1. Marras, I. S.; Zuburtikudis, I.; Panayiotou, C. Eur Polym J 2007, 43, 2191.
2. Shibata, M.; Someya, Y.; Orihara, M.; Miyoshi, M. J Appl Polym Sci 2006, 99, 2594.
3. Maiti, P.; Yamada, K.; Okamoto, M.; Ueda, K.; Okamoto, K. Chem Mater 2002, 14, 4654.
4. Hasook, A.; Tanoue, S.; Iemoto, Y. Polym Eng Sci 2006, 46, 1001.
5. Ray, S. S.; Okamoto, M. Prog Polym Sci 2003, 28, 1539.
6. Pogodina, V. N.; Cerclé, C.; Avérous, L.; Thomann, R.; Bouquey, M.; Muller, R. 4th Annual European Rheology Conference (AERC); Naples, Italy, 2007.
7. Cava, D.; Gimeonez, E.; Gavara, R.; Lagaron, M. J. J Plastic Film Sheeting 2006, 22, 265.
8. Ray, S. S.; Okamoto, M. Macromol Mater Eng 2003, 288, 936.
9. Ray, S. S.; Yamada, K.; Okamoto, M.; Ueda, K. Macromol Mater Eng 2003, 288, 203.
10. Nam, Y. J.; Ray, S. S.; Okamoto, M. Macromolecules 2003, 36, 7126.
11. Rhim, W. J.; Hong, I. S.; Ha, S. C. Food Sci Technol 2009, 42, 612.
12. Krikorian, V.; Pochan, J. D. Macromolecules 2009, 38, 6520.
13. Pluta, M. Polymer 2004, 45, 8239.
14. Ogata, N.; Jimenez, G.; Kawai, H.; Ogihara, T. J Polym Sci Part B: Polym Phys 1997, 35, 389.
15. Ray, D.; Sengupta, S.; Sengupta, S. S.; Mohanty, A.; Misra, M. Macromol Mater Eng 2006, 291, 1513.
16. Wu, M. T.; Wu, C. Y. Polym Degrad Stab 2006, 91, 2198.
17. Revol, J. F.; Dietrich, A.; Goring, D. A. I. Can J Chem 1987, 65, 1724.
18. Wang, S.; Cheng, Q.; Rials, G. T.; Lee, H. S. Proceedings of the Pacific Rim Bio-Based Composites Symposium; 20–23 November 2006, Kuala Lumpur, Malaysia.
19. Fukushima, K.; Tabuani, D.; Camino, G. Mater Sci Eng 2009, 29, 1433.
20. Reiter, G.; Sommer, U. J. J Chem Phys 2000, 112, 4376.
21. Haidong, L.i; Wei, N.; Chang, D.; Xiangling, J. Eur Polym J 2009, 45, 123.